Pretreatment mechanism of *β*-O-4 lignin during phosphoric acid-acetone process based on density functional theory and molecular dynamic simulations

Zhang Junjiao, Zhu Jinqi, Lin Changfeng, Wang Tipeng, Dong Changqing, Qin Wu[*]

(*National Engineering Laboratory for Biomass Power Generation Equipment, School of Renewable Energy,*
North China Electric Power University, Beijing 102206, China)

Abstract: Pretreatment mechanism of *β*-O-4 lignin ($L_{\beta\text{-O-4}}$) during the phosphoric acid-acetone process involves a series of interactions between lignin and solvent molecule (H_2O, CH_3COCH_3 and H_3PO_4) which lead to the adsorption, solubility and decomposition of lignin. Coniferyl alcohol guaiacyl glycerol (CAGG) with the predominant linkage (*β*-O-4 ether bond) was chosen as the model *β*-O-4 lignin ($L_{\beta\text{-O-4}}$) for investigating the detailed pretreatment mechanism based on density functional theory calculations and molecular dynamic simulations. Interactions between *β*-O-4 lignin and solvent molecules were firstly detected. Only physical interaction occurred between *β*-O-4 lignin and the solvent molecule. The attractive van der Waals interaction favored CH_3COCH_3 molecules approaching to $L_{\beta\text{-O-4}}$, showing a compatibility of $L_{\beta\text{-O-4}}$ in CH_3COCH_3 solution. Furthermore, following the temperature effect on the dynamics processes, larger dynamics calculations and experiments were carried out to reveal the detailed dissolution and precipitation of *β*-O-4 lignin in various solutions.

Keywords: lignin, lignocellulose, biomass, pretreatment, density functional theory (DFT)

DOI: 10.3965/j.ijabe.20160902.2212

1 Introduction

Lignin, an essential aromatic biopolymer responsible for the strength and shape of plants, comprises 15%-20% of lignocellulose[1]. Its abundance in nature, low weight, environmental friendliness, as well as its antioxidant, antimicrobial, and biodegradable nature, along with its

CO_2 neutrality and reinforcing capability, make it an ideal candidate for the development of novel polymer composite materials[2-9]. While various pretreatment methods including physical, chemical and biological approaches have been developed to extract lignin from lignocellulosic biomass, chemical-based pretreatments are the most promising for mass production[10,11].

An earlier report indicated the existence of a positive correlation between lignin S/G ratio (S = syringyl-like lignin structures; G = guaiacyl-like lignin structures) and cellulose biodegradability related to lignin depolymerization efficiency during chemical pulping[12]. Variations in the S/G ratio influence crosslinking between lignin and other cell wall components, which in turn modifies the microscopic structure and topochemistry of the cell wall. Lignins have been isolated from lignocelluloses at the initial organosolv (ethanol and diluted acid) pretreatment stage, which then migrate to the biomass surface[13]. Following migration, lignins

redistributed onto the surface and form droplets. During dilute acid pretreatment, with a temperature increase over the range of the lignin phase transition, the lignins coalesce into larger molten bodies. Afterward, lignin migrates out of the cell wall and is re-deposited on the plant cell surface[14]. Acid-catalyzed β-O-4 ether bond cleavage is accompanied by comprehensive condensation and demethoxylation reactions with increasing severity[15].

Ionic liquid pretreatment of eucalyptus and switchgrass shows that both S-lignin and G-lignin break down at high pretreatment temperatures (463 K), and neither S-lignin nor G-lignin in switchgrass break down at lower pretreatment temperatures (393 K)[16]. We obtained similar results in our previous work, where the S/G ratio increased from 0.56 to 1.06 and the CrI index decreased from 39.9% to 27.7% after phosphoric acid fractionation[17]. Phosphoric acid-acetone pretreatment has been found to be an effective pretreatment method for the extraction of lignin from lignocellulosic biomass[18]. However, the detailed interaction properties between lignin and solution related to the phosphoric acid-acetone pretreatment processes are still obscure.

Recently, computational tools have been employed to investigate bond-breaking of lignin during degradation[19-28], the coupling of monolignols[29-33], mechanical properties[34] and conversion[35-37]. In reference to these theoretical works, coniferyl alcohol guaiacyl glycerol (CAGG) was selected as the model β-O-4 lignin ($L_{\beta\text{-O-4}}$) to do theoretical calculations to investigate the detailed interaction between β-O-4 lignin and solvent molecules (H_3PO_4, H_2O, and CH_3COCH_3) based on the combination of density functional theory (DFT) calculations and molecular dynamic (MD) simulations. Results reveal the intrinsic correlation between the properties of $L_{\beta\text{-O-4}}$ and its behavior in H_2O, CH_3COCH_3 and H_3PO_4 related to the phosphoric acid-acetone pretreatment processes.

2 Methods

2.1 Models

Lignin contains multiple substructures repeated randomly, with the β-O-4 bond being predominant[38]. Coniferyl alcohol guaiacyl glycerol (CAGG) model is representative of β-O-4 ether linkages. In reference to the work of Haensel et al.[39], CAGG was modeled to do geometric optimization. The stable configuration is shown in Figure 1. The lignin model was optimized in different solutions by using a solvation model with the appropriate dielectric constant, ε, which is 1, 80.1, 20 and 12.7 for gas phase, water, acetone, and 85% w/w phosphoric acid solution, respectively, according to the work of Wang and Anderko[40] and Munson[41]. Specific interactions between lignin and the solvent molecules were not considered in this study, since the solvent is represented by a polarizable continuum with a particular dielectric constant. The absolute errors in bond lengths with respect to the equilibrium geometrical parameters were less than 0.1 Å. During geometric optimization, all atoms in these models were allowed to relax freely.
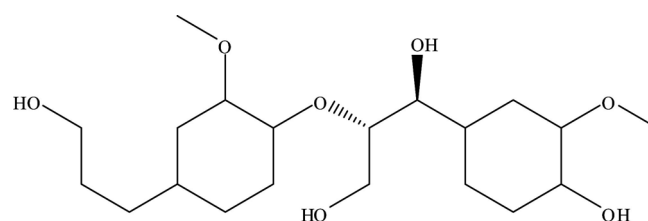

Figure 1　Diagram of the common CAGG model

We combined molecular dynamic (MD) simulations and density functional theory (DFT) calculations to study the relaxation process of $L_{\beta\text{-O-4}}$-H_2O, $L_{\beta\text{-O-4}}$-CH_3COCH_3, and $L_{\beta\text{-O-4}}$-H_3PO_4 interaction systems and their detailed electronic properties. A non-periodical amorphous with one $L_{\beta\text{-O-4}}$ and one solvent molecule (H_2O, CH_3COCH_3, and H_3PO_4) was built using a random method to perform MD simulations to obtain the equilibrium structure. Then, DFT calculations were performed to optimize the equilibrium $L_{\beta\text{-O-4}}$-H_2O, $L_{\beta\text{-O-4}}$-CH_3COCH_3 and $L_{\beta\text{-O-4}}$-H_3PO_4 structures for detecting the related detailed electronic properties. With these detailed electronic properties in mind, we built three-dimensional periodical systems consisting of one $L_{\beta\text{-O-4}}$ molecule and 100 solvent molecules (H_2O, CH_3COCH_3 and H_3PO_4) to investigate intermolecular force, and built larger three-dimensional periodical systems to study the relaxation process of a cluster of four $L_{\beta\text{-O-4}}$ segments dissolving or precipitating in the aqueous solution, acetone solution and phosphoric solution, respectively. Furthermore, the chemical stability of lignin in these various solutions was estimated

using DFT calculations.

2.2   MD simulations

The MD simulations were performed using the Discover module with a Compass force field at an NVT ensemble[42].   Energy minimizations were performed with a convergence criterion of 0.001 kcal/mol using a combination of the steepest descent and a conjugate gradient method of 100 steps each; these steps were repeated until satisfactory conformational parameters were obtained.   The time step was 1 fs, to integrate Newton's equation of motion.   A non-bonded cut-off of 10 Å was applied to truncate long-range interactions and increase computation speed, and the particle-mesh Ewald method (PME) algorithm with cubic-spline interpolation (1-Å grid width) was applied to efficiently calculate electrostatic interactions[43].

The potential function is a simple, empirically-derived mathematical expression that gives the energy of the interaction system as a function of the positions of the atoms, which can be calculated using the following potential energy function[44], as Equation (1):

$$U = \sum_{Bonds} K_b^i (b_i - b_0^i)^2 + \sum_{\substack{Bond \\ angles}} K_\theta^i (\theta_i - \theta_0^i)^2 +$$

$$\sum_{\substack{Torsion \\ angles}} K_\phi^i \{1 - \cos[n^i (\phi_i - \phi_0^i)]\} +$$

$$\sum_{\substack{Nonbonded\_pairs\_i,j \\ closer\_than\_cutoff}} [A_{sc}\varepsilon^{ij}(r_0^{ij}/r_{ij})^{12} - 2\varepsilon^{ij}(r_0^{ij}/r_{ij})^6 - \quad (1)$$

$$S_{vdw}(r_{ij})] + 332 \sum_{\substack{Partial\_charges \\ closer\_thann\_cutoff}} [q^i q^j/r_{ij} - S_{els}^A(r_{ij})]$$

The potential energy function is contributed by bonded interactions, bond angle bending, dihedral (or torsion) angle twisting, van der Waals interactions, and Coulomb interactions, are described by the 1st, 2nd, 3rd, 4th and the 5th term, respectively.   As described in the work of Qin et al.[45], each term can be estimated using different parameters.   The 1st term describes the bonded interactions acting between atoms separated by one covalent bond and the quadratic potential represents bond length stretching.   In the 1st term, b_i is the ith bond length and K_b^i is the force constant, the energy is at a minimum when b_i has the equilibrium value b_0^i.   The 2nd term describes bond angle bending and takes the same form as bond length stretching.   The 3rd term dihedral (or torsion) angle twisting is represented by cosine

function with a periodicity n^i and an equilibrium value at φ_0^i, where $2K_\varphi^i$ is the rotation barrier height.   The 4th term van der Waals interactions are represented by the Lennard-Jones 6-12 potential, the value of which depended on the terms $A_{sc}\varepsilon^{ij}(r_0^{ij}/r^{ij})^{12}$, $-2\varepsilon^{ij}(r_0^{ij}/r^{ij})^6$, and $-S_{vdw}(r_{ij})$. $\varepsilon^{ij}(r_0^{ij}/r^{ij})^{12}$ for the increasing repulsion as the electron clouds of atoms overlap; where A_{sc} is a scale factor used to reduce the van der Waals repulsion to compensate for the reduced attraction caused by truncation, $-2\varepsilon^{ij}(r_0^{ij}/r^{ij})^6$ is for the weak dispersion attraction that exists between all atoms, and r_{ij} is distance between atoms.   The 5th term Coulomb electrostatic potential is based on $q^i q^j/r_{ij}$, where $q_i q_j$ are charges of atoms.   Two shifting functions, $S_{vdw}^A(r_{ij})$ and $S_{els}^A(r_{ij})$, are introduced to compensate for the long-range interaction at a cutoff distance of r_c.   In contrast to the bonded interaction close to their equilibrium values, the nonbonded interactions are very important for simulations of biomolecules because of their great multiplicity.

2.3   DFT calculations

The DFT calculations were performed using the DMol³ program in the Accelrys Materials Studio software. The exchange-correlation energy of electrons was calculated with the spin-polarized generalized gradient approximation[46], as implemented in the DMol³ program. The Perde-Burke-Ernzerhof (PBE) exchange-correction functional[47,48] and the double numerical plus polarization (DNP)[49-51] basis set, which is equivalent in accuracy to the commonly-used 6-31G** Gaussian orbital basis set, were used throughout the calculations. However, the numerical basis set is much more accurate than a Gaussian basis set of the same size.   During the calculations, all atoms were relaxed and Brillouin zone integration was performed at the gamma point[52]. Calculations used an energy convergence tolerance of 1×10^{-6} Ha and a gradient convergence of 1×10^{-6} Ha/Å. A new formulation for the linear (LST) and quadratic synchronous transit (QST) methods was utilized to search the transition states and investigate lignin fragment decomposition[53].

3   Results and discussion

3.1   Interaction between $L_{\beta\text{-}O\text{-}4}$ and solvent molecule

We theoretically analyzed the interactions between

$L_{\beta\text{-O-4}}$ and the solvent molecules (H_2O, CH_3COCH_3 and H_3PO_4) by approaching the solvent molecule near to the $L_{\beta\text{-O-4}}$ to perform MD simulation to obtain the equilibrium structures, which were further geometrically optimized using DFT calculations. The stable interaction configurations are illustrated in Figure 2.
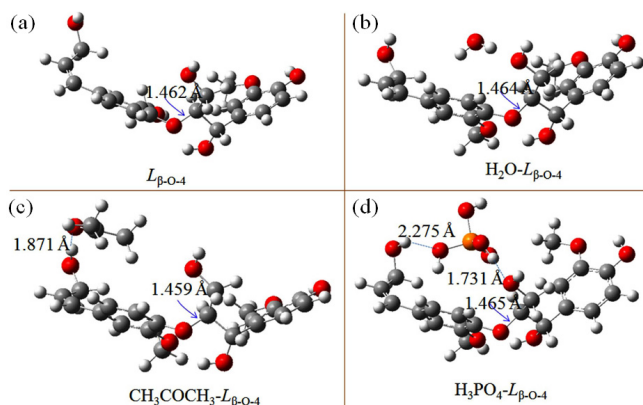

Figure 2   Stable configurations for (a) $L_{\beta\text{-O-4}}$ in the gas phase; (b) $L_{\beta\text{-O-4}}$-H_2O; (c) $L_{\beta\text{-O-4}}$-CH_3COCH_3 and (d) $L_{\beta\text{-O-4}}$-H_3PO_4

The binding energies, E_B, for the studied systems are calculated using Equation (2):

$$E_B = E(L_{\beta\text{-O-4}}\text{-solvent}) - E(L_{\beta\text{-O-4}}) - E(\text{solvent}) \qquad (2)$$

where, $E(L_{\beta\text{-O-4}}\text{-solvent})$ is the total energy for the $L_{\beta\text{-O-4}}$-solvent adsorption system; $E(L_{\beta\text{-O-4}})$ is the total energy for $L_{\beta\text{-O-4}}$, and $E(\text{solvent})$ is the total energy for the solvent molecule (H_2O, CH_3COCH_3 and H_3PO_4).

Table 1 lists the E_B calculated for the different $L_{\beta\text{-O-4}}$-solvent configurations shown in Figure 2. E_B for the $L_{\beta\text{-O-4}}$-H_2O case, $L_{\beta\text{-O-4}}$-CH_3COCH_3 case and $L_{\beta\text{-O-4}}$-H_3PO_4 case is −0.43 eV, −0.38 eV and −1.22 eV, respectively. Because of the polar groups of H_3PO_4 and two hydrogen bonds (with the length of 2.275 Å and 1.731 Å, respectively) make the interaction between $L_{\beta\text{-O-4}}$ and H_3PO_4 stronger than the $L_{\beta\text{-O-4}}$-H_2O and $L_{\beta\text{-O-4}}$-CH_3COCH_3 interaction cases. However, only physical interaction occurs between $L_{\beta\text{-O-4}}$ and the solvent molecule.

Table 1 E_B for the   three $L_{\beta\text{-O-4}}$-solvent configurations

	$L_{\beta\text{-O-4}}$-H_2O	$L_{\beta\text{-O-4}}$-CH_3COCH_3	$L_{\beta\text{-O-4}}$-H_3PO_4
E_B (eV)	−0.43	−0.38	−1.64

To further understand the interactions between lignin and solvent molecules, one $L_{\beta\text{-O-4}}$ and 100 solvent molecules (H_2O, CH_3COCH_3 and H_3PO_4) were filled into a box (100 Å × 100 Å × 100 Å) to perform MD simulations. Figure 3a depicts the related equilibrium structures for the simulated $L_{\beta\text{-O-4}}$-H_2O, $L_{\beta\text{-O-4}}$-CH_3COCH_3, and $L_{\beta\text{-O-4}}$-H_3PO_4 interaction systems. For the $L_{\beta\text{-O-4}}$-H_2O interaction system, three H_2O molecules approached the three OH groups of $L_{\beta\text{-O-4}}$, forming three hydrogen bonds. For the $L_{\beta\text{-O-4}}$-CH_3COCH_3 system, $L_{\beta\text{-O-4}}$ is coated by about 30 CH_3COCH_3 molecules. For the $L_{\beta\text{-O-4}}$-H_3PO_4 interaction system, only one H_3PO_4 molecule approached $L_{\beta\text{-O-4}}$, and H_3PO_4 molecules bound to each other by hydrogen bonds into several clusters far away from the surface of $L_{\beta\text{-O-4}}$. $L_{\beta\text{-O-4}}$ is hydrophobic (which corresponds to the previous work[54]), and is highly "acetone-philic". These phenomena should have significant relation to the van der Waals interactions between $L_{\beta\text{-O-4}}$ and solvent molecules. As shown in Figure 3b, with MD processes, the van der Waals energy is positive for the $L_{\beta\text{-O-4}}$-H_2O and $L_{\beta\text{-O-4}}$-H_3PO_4 interaction systems, while it is negative for the $L_{\beta\text{-O-4}}$-CH_3COCH_3 system. Therefore, similar to PE or PE-like polymers[55,56], the main driving force for CH_3COCH_3 adsorption and its orientation on $L_{\beta\text{-O-4}}$ is the attractive van der Waals interactions rather than chemical binding energy, which can be further explained by analyzing the density of state (DOS).
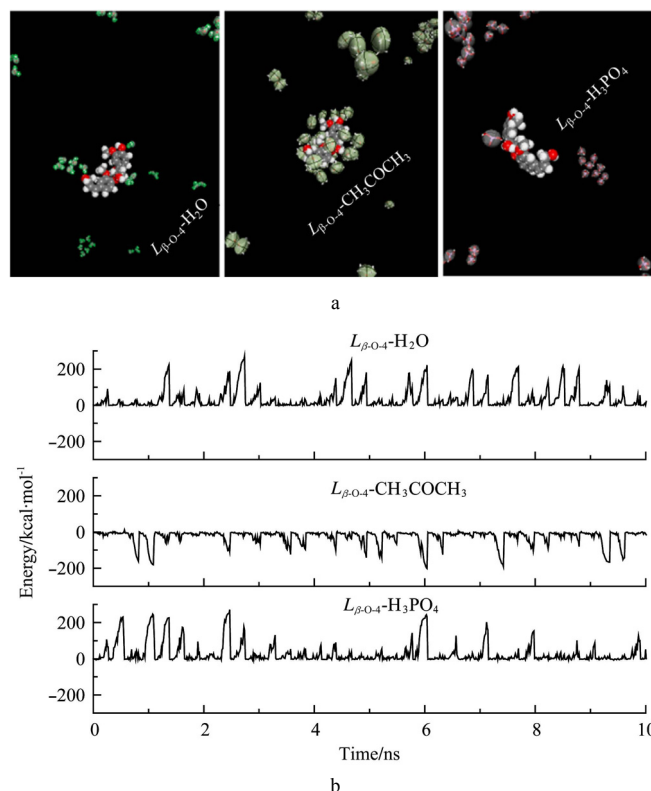

Figure 3   (a) Equilibrium structures and (b) time evolution of van der Waals energy for $L_{\beta\text{-O-4}}$-H_2O, $L_{\beta\text{-O-4}}$-CH_3COCH_3, and $L_{\beta\text{-O-4}}$-H_3PO_4 interaction systems

Figure 4 depicts the DOS for $L_{β\text{-O-4}}$ in the Equilibrium structures (Figure 3a). According to Figure 4, DOS for the pure $L_{β\text{-O-4}}$ is similar to those for $L_{β\text{-O-4}}$ in the equilibrium structures, which discuss the DOS for $L_{β\text{-O-4}}$ that interacts to one or more solvent molecule.
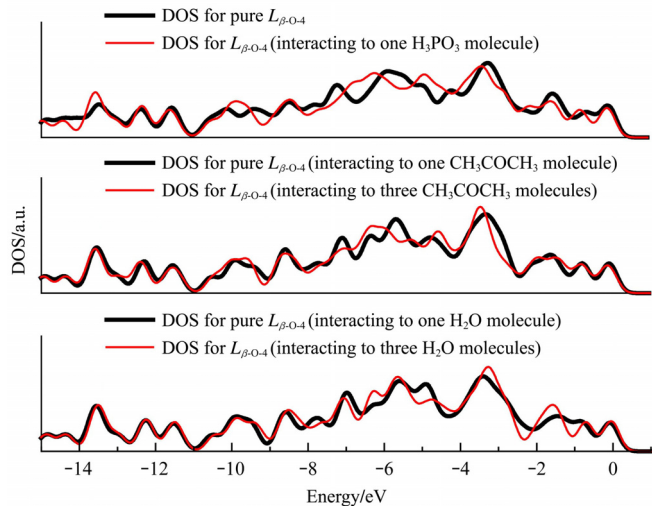

Figure 4   DOS for the pure $L_{β\text{-O-4}}$ and the $L_{β\text{-O-4}}$ interacting to one or more solvent molecule

3.2   Effect of temperature on *β*-O-4 Lignin in various solutions

Because lignin dissolution is temperature-dependent[57], the effect of temperature on the interaction between *β*-O-4 lignin and the solvent molecule was discussed. Figure 5 shows the potential energy as a function of time for NVT simulations at various temperatures over 40 ns. The potential energy for the $L_{β\text{-O-4}}$-H_2O interaction system is mainly contributed by the negative electrostatic interaction energy, while the van der Waals interaction energy is positive, reaching its maximum value of −50 kcal/mol at 283 K after about 20 ns. For the $L_{β\text{-O-4}}$-CH_3COCH_3 interaction system, the maximum potential energy is mainly contributed by the negative van der Waals interaction energy and the electrostatic interaction energy. Low temperature promotes the interaction between $L_{β\text{-O-4}}$ and CH_3COCH_3. For the $L_{β\text{-O-4}}$-H_3PO_4 interaction system, the temperature of about 383 K favors the interaction between $L_{β\text{-O-4}}$ and H_3PO_4, and this interaction is mostly caused by the negative electrostatic interaction, resulting in the maximum potential energy value of about −330 kcal/mol. According to temperature effect on the interactions between $L_{β\text{-O-4}}$ and the solvent molecule, a multi-stage

temperature control in various solutions could be expected for obtaining or removing lignin from the pretreatment process of lignocellulose.
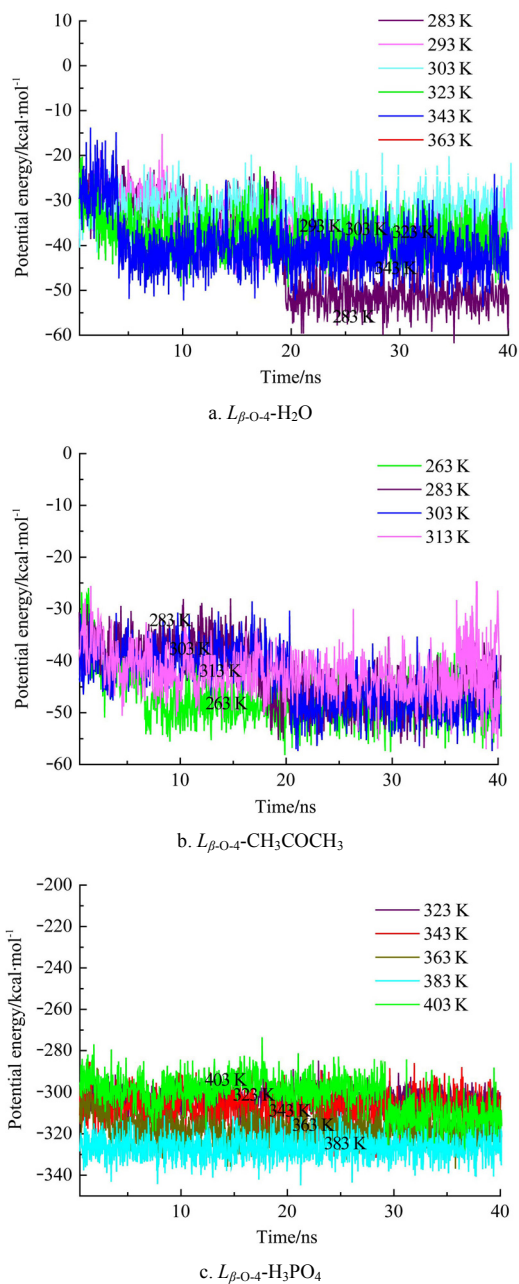

a. $L_{β\text{-O-4}}$-H_2O

b. $L_{β\text{-O-4}}$-CH_3COCH_3

c. $L_{β\text{-O-4}}$-H_3PO_4

Figure 5   Potential energy as a function of time at different temperatures for (a) $L_{β\text{-O-4}}$-H_2O; (b) $L_{β\text{-O-4}}$-CH_3COCH_3; and (c) $L_{β\text{-O-4}}$-H_3PO_4 interaction systems

3.3   Dissolution and precipitation of *β*-O-4 lignin in various solutions

MD simulations for larger $L_{β\text{-O-4}}$–solvents systems were performed to elucidate the interaction mechanisms between lignin and solvent molecule. Based on the relatively optimized temperature analyzed above, aqueous solution with 24000 water molecules and one lignin cluster (made up of three fragments of $L_{β\text{-O-4}}$) was defined

in the box (89.543 Å × 89.543 Å × 89.543 Å) to perform 10 ns MD simulation under 283 K, the results of which are presented in Figure 6a. CH_3COCH_3 solution with 3000 CH_3COCH_3 molecules and three fragments of $L_{\beta-O-4}$ was defined in the box of 71.61 Å × 71.61 Å × 71.61 Å. 10 ns MD simulation at 263 K was performed and the results were gathered in Figure 6b. Concentrated H_3PO_4 with 4416 H_3PO_4 molecules, 6400 water molecules, and one lignin cluster (made up of three fragments of $L_{\beta-O-4}$) is defined in the box of 81.05 Å × 81.05 Å × 81.05 Å, and the related 10 ns MD simulation results under 383 K are illustrated in Figure 6c.

For the MD process of $L_{\beta-O-4}$–H_2O solution system under 283 K, three separated $L_{\beta-O-4}$ fragments changed into an accumulation state after the 2 ns, while the $L_{\beta-O-4}$–CH_3COCH_3 solution system under 263 K showed the dissolution of the lignin segments where the three $L_{\beta-O-4}$ fragments separated into the CH_3COCH_3 solvent quickly after 1 ns. However, in phosphoric acid solution, the three lignin fragments were clearly twisted to each other a around the equilibrium state but still in an aggregation state after 10 ns of the MD process.

Both the entropy and the enthalpy of the $L_{\beta-O-4}$–H_2O solution system diminished, and the absolute value |ΔH| was much higher than |ΔS|, resulting in $\Delta G = \Delta H – T\Delta S < 0$. Thus, a spontaneous precipitation phenomenon can be observed with the formation of hydrogen bonds between each $L_{\beta-O-4}$ fragment, as shown in Figure 6a, with the flocculated lignin cluster heterogeneously distributed in the solution[58].   For the $L_{\beta-O-4}$–CH_3COCH_3 solution system, the enthalpy decreased in this course chiefly because of van der Waals interactions, while the entropy increased, especially in the solution system, so that $\Delta G = \Delta H – T\Delta S < 0$. Hence, external force or energy was unnecessary to dissolve lignin in the CH_3COCH_3 solution with the breaking of hydrogen bonds inside the lignin cluster, and acetone-soluble lignin was generated[59]. However, the entropy of the $L_{\beta-O-4}$–H_3PO_4 solution system diminished, while the enthalpy changed slightly, which therefore resulted in $\Delta G \leq 0$. The hydrogen bonds between $L_{\beta-O-4}$ made the three $L_{\beta-O-4}$ segments firmly bind to each other in the $L_{\beta-O-4}$–H_3PO_4 solution system even under a longer MD process. Hydrogen bond contributed

greatly to the arrangement of β-O-4 lignin in various solutions, where the solvent can either promote the formation of hydrogen bonds to bind the $L_{\beta-O-4}$ fragments to each other, or break the hydrogen bonds to separate the $L_{\beta-O-4}$ fragments from each other leading to the dissolution of β-O-4 lignin.
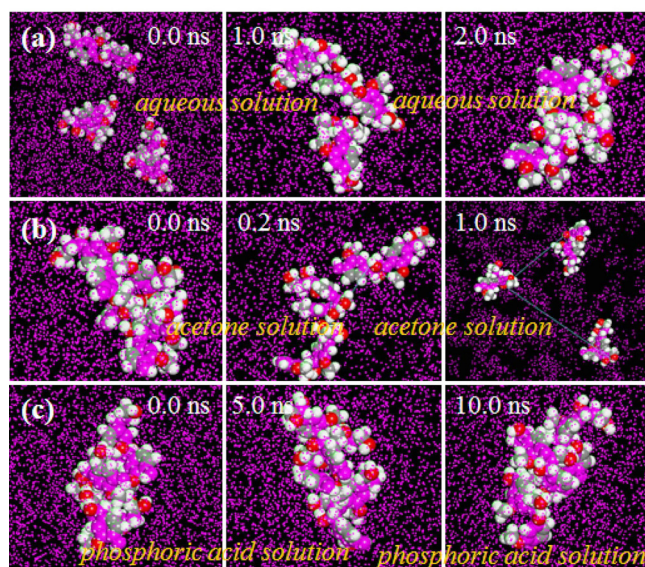

Figure 6   Conformations of lignin in (a) aqueous, (b) acetone and (c) phosphoric acid solutions after MD simulations

3.4   Chemical stability of lignin in various solutions

To understand the chemical stability of lignin in various solutions, we calculated the barrier energy needed for the breakage of the inner β-O-4 bond between the aromatic rings.   Figure 7a depicts the calculated potential energy profiles for the decomposition reaction of $L_{\beta-O-4}$ in aqueous solution.   The reaction initiated from the optimized geometry of $L_{\beta-O-4}$ in aqueous solution. The energy barrier (E_a) and the reaction energy (E_r) are 2.398 eV and 2.350 eV, respectively.   The breakage of β-O-4 is an endothermic process with the E_a far higher than 0.75 eV (a magnitude regarded as surmountable for reactions occurring at room temperatures), which imply that the reaction is energetically close.   Figure 7b displays the same energy profiles as Figure 7a, but for the decomposition of $L_{\beta-O-4}$ in acetone solution.   The endothermic one-step reaction process in acetone solution is also energetically close with the E_a of 2.627 eV and E_r of 2.328 eV.   In Figure 7c, the one-step decomposition reaction in phosphoric acid solution initiated from the initial state (IS), crossed the energy of 2.415 eV at the transition state (TS), and then turned into the final state

(FS).   The reaction energy is 2.398 eV.   Comparing these energy profiles, we found that $L_{\beta\text{-O-4}}$ was chemically stable in the three solutions and the stability of $L_{\beta\text{-O-4}}$ in solution following the order acetone solution, phosphoric acid solution, and aqueous solution.

The highest occupied molecular orbital (HOMO) mediates the hole transfer through biomaterials, and the lowest unoccupied molecular orbital (LUMO) mediates the electron transfer.   Therefore, HOMO and LUMO are of importance to characterize the chemical stability and activity of the critical points, *i.e.* IS, TS and FS in different solutions.   According to Figure 7, one aromatic ring of $L_{\beta\text{-O-4}}$ contributes to the HOMO and the other aromatic ring contributes to the LUMO of the IS.   Then, in comparison with the IS, partial hole and electron transport to the opposite aromatic ring, implying the bridge effect of the *β*-O-4 linkage.   After the completely break of the *β*-O-4 linkage of $L_{\beta\text{-O-4}}$ into FS, electron and charge transfer to the opposite aromatic ring while compared to the IS in the acetone and phosphoric acid solutions.   Comparing the HOMO and LUMO of $L_{\beta\text{-O-4}}$ in aqueous solution, acetone solution, and phosphoric acid solution, we find that, at the IS, LUMO of $L_{\beta\text{-O-4}}$ in both aqueous and phosphoric acid solutions is far more obvious than that in acetone solution, which suggests that acetone makes it relatively difficult to excite electron of atoms in one aromatic ring of $L_{\beta\text{-O-4}}$ and then transport through the linkage to atoms in the other aromatic ring. The electronic properties would be related to the higher E_a of $L_{\beta\text{-O-4}}$ decomposition in acetone solution than those in both aqueous and phosphoric acid solutions. Moreover, HOMO and LUMO distributions of $L_{\beta\text{-O-4}}$ at IS, FS and TS in aqueous solution make electron and hole transfer easier than in acetone and phosphoric acid solutions.   Therefore, aqueous solution reduces the E_a of $L_{\beta\text{-O-4}}$ decomposition.   The hole and electron transport analysis characterize the importance of *β*-O-4 linkage in $L_{\beta\text{-O-4}}$, which, together with the modification of frontier orbital of $L_{\beta\text{-O-4}}$, throws light deep into the chemical stability of $L_{\beta\text{-O-4}}$ in different solution.

Real lignin structure is far more complicated than $L_{\beta\text{-O-4}}$, but this work reveals the detailed property and solubility of $L_{\beta\text{-O-4}}$ in various solutions, providing a fundamental understanding for the pretreatment process of lignin during phosphoric acid-acetone process.
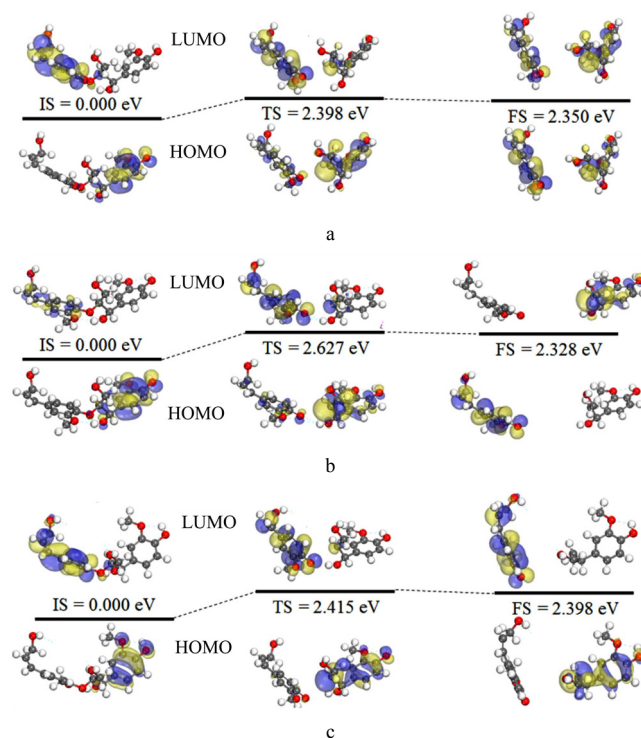

Figure 7   Energy profile for the decomposition of $L_{\beta\text{-O-4}}$ with the isosurface (0.03) of HOMO and LUMO in (a) aqueous solution, (b) acetone solution and (c) phosphoric acid solution.   The initial state, transition state, and final state are denoted as IS, TS and FS, respectively

3.5   Experimental control

Referring to our previous work[17,60], we pretreated Chinese white poplar using the phosphoric acid-acetone method under modest reaction conditions.   The feedstock and phosphoric acid (85 wt.%) with the ratio of 1:8 (m/v, g/mL) were mixed into slurry at 110°C under vigorous stirring for 1 h.   Then acetone was introduced to sufficiently precipitate the slurry.   After filtration and being washed with water, the solid obtained was dried at 4°C under vacuum.   The phosphoric acid-acetone pretreatment could conserve 96% cellulose and remove more than 50% lignin, hemicellulose dissolved into the mixed rinsing liquid in the form of monomeric xylose. The experiment performed under the theoretically optimized pretreatment temperature increases the efficiency of lignin removal by 10% in comparison with the results reported in our previous work[17,60].   Then, better separation of lignin from cellulose will lead to more efficient hydrolyzation of cellulose by cellulase enzyme.

4   Conclusions

A combination of density functional theory (DFT) calculations and molecular dynamic (MD) simulations at the molecule level was performed to detect the detailed interactions between β-O-4 lignin ($L_{\beta\text{-O-4}}$) and the solvent molecule (H_2O, CH_3COCH_3 and H_3PO_4) related to pretreatment of lignin during phosphoric acid-acetone process.   Physical interaction happens between $L_{\beta\text{-O-4}}$ and solvent molecules, as was observed in terms of binding energy values.   The CH_3COCH_3 shortened the β-O-4 bond length, while H_2O and H_3PO_4 lengthened the β-O-4 bond length.   The van der Waals energies for the $L_{\beta\text{-O-4}}$-H_3PO_4 and $L_{\beta\text{-O-4}}$-H_2O system are positive, while it is negative for the $L_{\beta\text{-O-4}}$-CH_3COCH_3 system.   The MD simulation procedures reveal   that CH_3COCH_3 breaks the hydrogen bonds inside the lignin clusters, leading to the dissolution of $L_{\beta\text{-O-4}}$.   The addition of H_2O results in the formation of hydrogen bonds between lignin fragments, flocculating the $L_{\beta\text{-O-4}}$ fragments.   Reaction active energies (E_a) for $L_{\beta\text{-O-4}}$ decomposition in aqueous solution, acetone solution, and phosphoric acid solution are around 2.5 eV, much higher than 0.75 eV, which implies that lignin is chemically stable in these solvents. The charge transport of lignin could be regulated using different solutions, and β-O-4 linkage plays an important role in the charge transport between rings of $L_{\beta\text{-O-4}}$. Furthermore, the experimental results of this study correspond to the theoretical results, where lignin swells and dissolves in CH_3COCH_3 at about 0°C, and the dissolved lignin flocculates with the addition of H_2O.

Acknowledgements

[References]

[1]   Pauly M, Keegstra K.   Cell-wall carbohydrates and their modification as a resource for biofuels.   Plant J., 2008; 54(4): 559−568.

[2]   Feldman D, Banu D, Manley R S J, Zhu H.   Highly filled blends of a vinylic copolymer with plasticized lignin: Thermal and mechanical properties.   J. Appl. Polym. Sci., 2003; 89(7): 2000−2010.

[3]   Erakovic S, Veljovic D, Diouf P N, Stevanovic T, Mitric M, Milonjic S, et al.   Electrophoretic deposition of biocomposite lignin / hydroxyapatite coatings on titanium. Inter. J. Chem. React. Eng., 2009; 7(1): 1542−6580.

[4]   Raschip I E, Hitruc E G, Vasile C.   Semi-interpenetrating polymer networks containing polysaccharides.   II. Xanthan/lignin networks: A spectral and thermal characterization.   High Perform. Polym., 2011; 23(3): 219−229.

[5]   Cerrutti B M, de Souza C S, Castellan A, Ruggiero R, Frollini E.   Carboxymethyl lignin as stabilizing agent in aqueous ceramic suspensions.   Ind. Crop. Prod., 2012; 36(1): 108−115.

[6]   Faria F A, Evtuguin D V, Rudnitskaya A, Gomes M T, Oliveira J A, Graca M P F, et al.   Lignin-based polyurethane doped with carbon nanotubes for sensor applications. Polym. Int., 2012; 61(5): 788−794.

[7]   Graça M P F, Rudnitskaya A, Faria F A C, Evtuguin D V, Gomes M T S R, Oliveira J A B P, et al.   Electrochemical impedance study of the lignin-derived conducting polymer. Electrochim. Acta, 2012; 76: 69−76.

[8]   Rozite L, Varna J, Joffe R, Pupurs A.   Nonlinear behavior of PLA and lignin-based flax composites subjected to tensile loading.   J. Thermoplast. Compos., 2013; 26(4): 476−496.

[9]   Wang H, Zou J, Shen Y, Fei G, Mou J.   Preparation and colloidal properties of an aqueous acetic acid lignin containing polyurethane surfactant.   J. Appl. Polym. Sci., 2013; 130(3): 1855−1862.

[10]   Li Z L, Ge Y.   Antioxidant activities of lignin extracted from sugarcane bagasse via different chemical procedures. Int J Biol Macromol., 2012; 51(5): 1116−1120.

[11]   Penkina A, Hakola M, Paaver U, Vuorinen S, Kirsimäe K, Kogermann K, et al.   Solid-state properties of softwood lignin and cellulose isolated by a new acid precipitation method.   Int J Biol Macromol., 2012; 51(5): 939−945.

[12]   Papa G, Varanasi P, Sun L, Cheng G, Stavila V, Holmes B, et al.   Exploring the effect of different plant lignin content and composition on ionic liquid pretreatment efficiency and enzymatic saccharification of *Eucalyptus globulus* L. mutants. Bioresource Technol., 2012; 117: 352−359.

[13]   Koo B W, Min B C, Gwak K S, Lee S M, Choi J W, Yeo H, et al.   Structural changes in lignin during organosolv pretreatment of Liriodendron tulipifera and the effect on enzymatic hydrolysis.   Biomass Bioenerg, 2012; 42: 24−32.

[14]   Donohoe B S, Decker S. R, Tucker M P, Himmel M E, Vinzant T B.   Visualizing lignin coalescence and migration

through maize cell walls following thermochemical pretreatment. Biotechnol. Bioeng., 2008; 101(5): 913−925.

[15] Wang K, Yang H, Yao X, Xu F, Sun R C. Structural transformation of hemicelluloses and lignin from triploid poplar during acid-pretreatment based biorefinery process. Bioresource Technol., 2012; 116: 99−106.

[16] Varanasi P, Singh P, Arora R, Adams D, Auer M, Simmons B A, et al. Understanding changes in lignin of Panicum virgatum and Eucalyptus globulus as a function of ionic liquid pretreatment. Bioresource Technol., 2012; 126: 156−161.

[17] Kang P, Zheng Z M, Qin W, Dong C Q, Yang Y P. Efficient fractionation of Chinese white poplar biomass with enhanced enzymatic digestability and modified acetone-soluble lignin. Bioresources, 2011; 6(4): 4705−4720.

[18] Zhang Y H P, Cui J B, Lynd L R, Kuang L R. A transition from cellulose swelling to cellulose dissolution by o-phosphoric acid: Evidence from enzymatic hydrolysis and supramolecular structure. Biomacromolecules, 2006; 7(2): 644−648.

[19] Beste A, Buchanan III A C Computational study of bond dissociation enthalpies for lignin model compounds. Substituent effects in phenethyl phenyl ethers. J. Org. Chem., 2009; 74(7): 2837−2841.

[20] Cho D W, Parthasarathi R, Pimentel A S, Maestas, G D, Park H J, Yoon U C, et al. Nature and kinetic analysis of carbon-carbon bond fragmentation reactions of cation radicals derived from SET-oxidation of lignin model compounds. J. Org. Chem., 2010; 75(19): 6549−6562.

[21] Elder T. Computational study of pyrolysis reactions of lignin model compounds. Holzforschung, 2010; 64(4): 435−440.

[22] Elder T. Bond dissociation enthalpies of a dibenzodioxocin lignin model compound. Energ. Fuel, 2013; 27(8): 4785−4790.

[23] Jarvis M W, Daily J W, Carstensen H-H, Dean A M, Sharma S, Dayton D C, et al. Direct detection of products from pyrolysis of 2-phenethyl phenyl ether. J. Chem. Phys. A., 2011; 115(4): 428−438.

[24] Kim S, Chmely S C, Nimlos M R, Bomble Y J, Foust T D, Paton R S, et al. Computational study of bond dissociation enthalpies for a large range of native and modified lignins. J. Phys. Chem. Lett., 2011; 2(22): 2846−2852.

[25] Parthasarathi R, Romero R A, Redondo A, Gnanakaran S. Theoretical study of the remarkably diverse linkages in lignin. J. Phys. Chem. Lett., 2011; 2(20): 2660−2666.

[26] Younker J M, Beste A, Buchanan III A C. Computational study of bond dissociation enthalpies for substituted β-O-4 lignin model compounds. ChemPhysChem., 2011; 12(18): 3556−3565.

[27] Younker J M, Beste A, Buchanan III A C. Computational study of bond dissociation enthalpies for lignin model compounds: β-5 arylcoumaran. Chem. Phys. Lett., 2012; 545: 100−106.

[28] Gardrat C, Ruggiero R, Rayez M-T, Rayez J-C, Castellan A. Experimental and theoretical studies of the thermal degradation of a phenolic dibenzodioxin lignin model. Wood Sci. Technol., 2013; 47(1): 27−41.

[29] Durbeej B, Eriksson L A. Formation of β-O-4 lignin models - A theoretical study. Holzforschung, 2003; 57(5): 466−478.

[30] Durbeej B, Eriksson L A. A density functional theory study of conferyl alcohol intermonomeric cross linkages in lignin-three-dimensional structures, stabilities and the thermodynamic control hypothesis. Holzforschung, 2003; 57(2): 150−164.

[31] Martínez C, Rivera J L, Herrera R, Rico J L, Flores N, Rutiaga J G, et al. Evaluation of the chemical reactivity in lignin precursors using the fukui function. J. Mol. Model., 2008; 14(2): 77−81.

[32] Shigematsu M, Masamoto H. Solvent effects on the electronic state of monolignol radicals as predicted by molecular orbital calculations. J. Wood Sci., 2008; 54(4): 308−311.

[33] Sangha A K, Parks J M, Standaert R F, Ziebell A, Davis M, Smith J C. Radical coupling reactions in lignin sythesis: A density functional theory study. J. Phys. Chem. B., 2012; 116(16): 4760−4768.

[34] Elder T. Quantum chemical determination of Young's modulus of lignin calculations on a *β*-O-4 model compound. Biomacromolecules, 2007; 8(11): 3619−3627.

[35] Holmelid B, Kleinert M, Barth T. Reactivity and reaction pathways in thermochemical treatment of selected lignin-like model compounds under hydrogen rich conditions. J. Anal. Appl. Pyrol., 2012; 98: 37−44.

[36] Chu S, Subrahmanyam A V, Huber G W. The pyrolysis chemistry of a *β*-O-4 type oligomeric lignin model compound. Green. Chem., 2013; 15(1): 125−136.

[37] Wu X, Fu J, Lu X. Kinetics and mechanism of hydrothermal decomposition of lignin model compounds. Ind. Eng. Chem. Res., 2013; 52(14): 5016−5022.

[38] Freudenberg K, Neish A C. Constitution and Biosynthesis of Lignin. New York: Springer-Verlag, 1968; 784p.

[39] Haensel T, Reinmöller M, Lorenz P, Beenken W J D, Krischok S, Ahmed S I U. Valence band structure of cellulose and lignin studied by XPS and DFT. Cellulose, 2012; 19(3): 1005−1011.

[40] Wang P, Anderko A. Computation of dielectric constants of solvent mixtures and electrolyte solutions. Fluid Phase

Equilibria, 2001; 186: 103−122.

[41] Munson R A. Dielectric constant of phosphoric acid. J. Chem. Phys. 1964; 40: 2044−2046.

[42] Phillips J C, Braun R, Wang W, Gumbart J, Tajkhorshid E, Villa E, et al. Scalable molecular dynamics with NAMD. J. Comput. Chem., 2005; 26(16): 1781−1802.

[43] Darden T, York D, Pedersen L. Particle mesh ewald: An N Log(N) method for Ewald sums in large systems. J. Chem. Phys., 1993; 98(12): 10089−10092.

[44] Levitt M, Hirshberg M, Sharon R, Daggett V. Potential energy function and parameters for simulations of the molecular dynamics of proteins and nucleic acids in solution. Comput. Phys. Commun., 1995; 91(1-3): 215−231.

[45] Qin W, Li X, Bian W W, Fan X J, Qi J Y. Density functional theory calculations and molecular dynamics simulations of the adsorption of biomolecules on graphene surfaces. Biomaterials, 2010; 31(5): 1007−1016.

[46] Perdew J P, Burke K, Wang Y. Generalized gradient approximation for the exchange-correlation hole of a many electron system. Phys. Rev. B 1996; 54(23): 16533−16539.

[47] Perdew J P, Burke K, Ernzerhof M. Generalized gradient approximation made simple. Phys. Rev. Lett., 1996; 77(18): 3865−3868.

[48] Perdew J P, Burke K, Ernzerhof M. Generalized gradient approximation made simple. Phys. Rev. Lett., 1997; 78(7): 396.

[49] Delley B. An all-electron numerical method for solving the local density functional for polyatomic molecules. J. Chem. Phys., 1990; 92(1): 508−517.

[50] Delley B. Fast calculation of electrostatics in crystals and large molecules. J. Phys. Chem., 1996; 100(15): 6107−6110.

[51] Delley B. From molecules to solids with the DMol3 approach. J. Phys. Chem., 2000; 113(18): 7756−7764.

[52] Kudin K N, Ozbas B, Schniepp H C, Prudhomme R K, Aksay I A, Car R. Raman spectra of graphite oxide and functionalized graphene sheets. Nano Lett., 2008; 8(1): 36−41.

[53] Govind N, Petersen M, Fitzgerald G, Smith D K, Andzelm J. A generalized synchronous transit method for transition state location. Comp. Mater. Sci., 2003; 28(2): 250−258.

[54] Nordström Y, Norberg I, Sjöholm E, Drougge R. A new softening agent for melt spinning of softwood kraft lignin. J. Appl. Polym. Sci., 2013; 129(3): 1274−1279.

[55] Zhang X B, Li Z S, Lu Z Y, Sun C C. Molecular dynamics simulation of the linear low-density polyethylene crystallization. J. Chem. Phys., 2001; 115(8): 3916−3922.

[56] Zhang X B, Li Z S, Yang H, Sun C C. Molecular dynamics simulations on crystallization of polyethylene copolymer with precisely controlled branching. Macromolecules, 2004; 37(19): 7393−7400.

[57] Norgren M, Edlund H, Lars W. Fundamental physical aspects on lignin dissolution. Nord. Pulp. Pap. Res. J., 2002; 17(4): 370−373.

[58] Fiţigău I F, Peter F, Boeriu C G. Structural analysis of lignins from different sources. World Academy of Science, Eng. Technol., 2013; 7: 98−103.

[59] Methacanon P, Weerawatsophon U, Thainthongdee M, Lekpittaya P, Kasetsart J. Optimum conditions for selective separation of kraft lignin. Kasetsart J. (Nat. Sci.), 2010; 44(4): 680−690.

[60] Kang P, Qin W, Zheng Z M, Dong C Q, Yang Y P. Theoretical study on the mechanisms of cellulose dissolution and precipitation in the phosphoric acid-acetone process. Carbohyd. Polym., 2012; 90(4): 1771−1778.